Chapter 4
Discriminating Properties of Alkali Metal Ions Towards the Constituents of Proteins and Nucleic Acids. Conclusions from Gas-Phase and Theoretical Studies

Mary T. Rodgers and Peter B. Armentrout

Contents

M.T. Rodgers (✉)
Department of Chemistry, Wayne State University, Detroit, MI 48202, USA
e-mail: mrodgers@chem.wayne.edu

P.B. Armentrout (✉)
Department of Chemistry, University of Utah, Salt Lake City, UT 84112, USA
e-mail: armentrout@chem.utah.edu

A. Sigel, H. Sigel, and R.K.O. Sigel (eds.), *The Alkali Metal Ions: Their Role for Life*,
Metal Ions in Life Sciences 16, DOI 10.1007/978-3-319-21756-7_4

Abstract Quantitative insight into the structures and thermodynamics of alkali metal cations interacting with biological molecules can be obtained from studies in the gas phase combined with theoretical work. In this chapter, the fundamentals of the experimental and theoretical techniques are first summarized and results for such work on complexes of alkali metal cations with amino acids, small peptides, and nucleobases are reviewed. Periodic trends in how these interactions vary as the alkali metal cations get heavier are highlighted.

Keywords Amino acids • Collision-induced dissociation • Infrared multiple photon dissociation • Nucleobases • Peptides

Please cite as: *Met. Ions Life Sci.* 16 (2016) 103–131

1 Introduction

Alkali cations interact with biological molecules via noncovalent, predominantly electrostatic interactions that are non-directional. In real biological systems, this means that the ion can interact with many components of its surroundings simultaneously. As a consequence, it is difficult to quantitatively characterize the strengths of such interactions. One means to overcome the lack of thermodynamic data on these systems is to examine models in the gas phase, where pairwise interactions between individual components of biological systems can be quantitatively measured with accuracy and precision. This can be achieved both for simple systems and for more complex interactions that evolve with larger systems. Coupled with an understanding of the detailed structure of these model complexes, such pairwise interactions can be used to provide estimates of the energetics of actual biological systems that can include subtle thermodynamic aspects of these complex systems. We have previously discussed the development of such a thermodynamic "*vocabulary*" for metal ion interactions in biological systems [1], which leads to the "*phrases, sentences, paragraphs, and book chapters*" that comprise real biological systems.

One strength of the relatively small gas-phase systems explored in this chapter is that the quantitative experimental information can be directly compared with high level theoretical results. Such comparisons play two equally important roles. First, they elucidate subtle features in the periodic trends in the metal cation affinities and how these vary with the properties of the biological molecules. It is the trends in these features (elucidated below) that transcend the gas-phase and allow application to condensed phase systems. Second, these comparisons provide important benchmarks to which levels of theory are useful approaches to describe such interactions and with what degree of accuracy.

2 Experimental and Theoretical Methods

Because alkali cations are naturally charged, their interactions with biomolecules are readily studied using a range of mass spectrometric (MS) techniques, which provide specificity regarding the identity of the complexes being studied. More advanced methods must be combined with MS in order to elucidate structure and thermodynamic information. In this section, we introduce the gas-phase experimental and theoretical methods that have been used to quantitatively explore the interactions of alkali metal cations with biomolecules. This section is designed to provide an overview of the methods along with appropriate literature references leading to more detailed expositions for the interested reader. The focus of this chapter is two experimental techniques, namely infrared multiple photon dissociation (IRMPD) and threshold collision-induced dissociation (TCID) utilized by the authors, but these approaches legitimately provide much of the available quantitative information on the systems of interest. Other useful experimental methods are also introduced.

2.1 Infrared Multiple Photon Dissociation Experiments

One means of providing structural information regarding gas-phase ions is to measure their infrared (IR) spectrum, either in the fingerprint region of 500 – 2000 cm^{-1} or in the hydrogen stretching region from 2800 – 3600 cm^{-1}. The difficulty with acquiring the desired IR spectrum for ions is that the concentrations of ions cannot easily be raised to the level needed for absorption measurements. Unlike solution phase species, where the concentration can be easily adjusted over a very wide range, the concentration of gas-phase ionic species is limited by the Coulombic repulsion between the ions. To overcome this limitation, several "action" spectroscopies have been developed in which the absorption of a photon (or multiple photons) induces dissociation, which is easily monitored using mass spectrometers. In a "tagging" infrared photodissociation experiment, a weakly bound species (usually a rare gas atom) is attached to the ion of interest. For such a molecular ion, absorption of a single IR photon is generally sufficient to cleave the noncovalent interaction with the tag.

Generation of such tagged molecules usually requires cryogenic conditions and the tagging atom may perturb the absorption spectrum. Alternatively, the ion can be probed directly if multiple photons are absorbed in an infrared multiple photon dissociation experiment. IRMPD requires only routine ion production methods but necessitates the use of higher powered lasers to provide sufficient fluence to allow absorption of multiple photons. Thus, the use of free electron lasers (FELs) has been commonplace in such studies, with facilities in the Netherlands (the Free Electron Lasers for Infrared eXperiments, FELIX) and France (Centre Laser Infrarouge d'Orsay, CLIO) being used extensively for such work.

Furthermore, the need for the absorption of multiple photons can distort the spectrum (often to the red to compensate for anharmonicity of vibrational modes). IRMPD generally relies on efficient intramolecular vibrational redistribution (IVR) [2, 3], which allows the ion to absorb a photon into a specific vibrational mode and then transfer that energy into other vibrational modes such that absorption of additional photons at the same photon frequency can occur again and again [4, 5]. IVR works best for larger ions with higher state densities. IRMPD studies of ions as small as four atoms have been conducted [6], but these required an intracavity laser (the Free Electron Laser for IntraCavity Experiments, FELICE, at the FELIX facility), where the photon flux is orders of magnitude higher than for an externally coupled laser.

Structural information for ions is generally obtained from IRMPD results by comparing the experimental spectrum with that generated from quantum chemical calculations (see Section 2.4). A major caveat is that the latter provides a prediction for absorption of a single photon, generally in the harmonic limit (although explicit anharmonic calculations are increasingly performed) [7–9]. Because of the multiple photon nature of the IRMPD spectrum, bands can be shifted according to the anharmonicity of the vibrational mode and intensities can vary appreciably (with weak bands showing little or no intensity because insufficient photons are absorbed to induce fragmentation). Nevertheless, the agreement between IRMPD and theoretical spectra is often sufficient for unequivocal identification of the conformation of the ion involved, even when multiple low-energy conformations may be present.

2.2 Collision-Induced Dissociation Experiments

Collision-induced dissociation (CID) experiments, also known as collisional activation (CA) or collision activated dissociation (CAD), take advantage of the fact that ions are charged and therefore easily accelerated to hyperthermal kinetic energies using electric fields. If these accelerated ions collide with an unreactive species (usually one of the rare gases but other gases or even surfaces can be used), translational to internal energy transfer occurs and provides sufficient internal energy to induce fragmentation. The extent of dissociation observed depends on the amount of energy transferred, the complexity of the ion, and the time scale over which the fragmentation is detected. In analytical applications, CID can be used to sequence complicated biomolecules (peptides, proteins, DNA, and RNA) simply by measuring the masses of fragment ions. Cleavage of various peptide (or phosphate ester) bonds along the backbone leads to a sequence of fragment ions that, if complete enough, enable the original primary structure of the biomolecule to be elucidated.

CID can also be used more quantitatively to measure the thermodynamics associated with the dissociations, so-called threshold CID experiments (TCID) [10]. In this application, ions are subjected to single collisions with an inert gas with the collision energy varied from zero through the energies needed to induce fragmentation. Analysis of the resultant kinetic energy-dependent processes reveals the threshold energy for the observed fragmentation pathways, which can be related to the heights of the rate-limiting transition states. Although tandem

mass spectrometers such as triple quadrupole MS (QQQ) can be used to provide such kinetic energy-dependent data, the best quantitative information is obtained using specialized instrumentation, notably a guided ion beam tandem mass spectrometer (GIBMS) [11]. This instrument is specifically designed for such quantitative studies and enables very low and well controlled collision energies and excellent collection of product ions.

Determination of the threshold energy in TCID experiments requires consideration of several experimental parameters including effects of multiple collisions [12], internal energy distributions [13], translational energy distributions [11], lifetimes for dissociation [14], competition between reaction channels [15], and sequential dissociations [16]. Methods for modeling all of these effects are detailed in the literature [17] and have proven to provide accurate thermodynamic information. Comparison of TCID results to quantities determined using equilibrium measurements (Section 2.3.1) of these quantities are generally in good agreement [18–24], although TCID has been applied to many systems where equilibrium methods are simply inaccessible. For such systems, comparison with theoretical information generally confirms the accuracy of TCID results.

It has also been realized that the thermochemistry derived from TCID measurements can be used for structural identification of fragment ions [25–30]. As for IRMPD studies, this is generally achieved by comparison of the experimental results with those derived from theory. TCID thermochemistry is insufficiently precise to distinguish between isomers or conformers that are relatively close in energy (whereas IRMPD can be very sensitive to such differences), but can be applied to fragment ions, which may not be generated in sufficient quantity to interrogate using IRMPD methods. Although different conclusions from these two approaches have been found [28, 31], they can be attributed to the harsher source conditions needed to generate sufficient ion intensities for IRMPD studies. In contrast, TCID is sensitive to the structure of the species formed at threshold, which is often but may not be the thermodynamically most favorable isomer.

2.3 Other Experimental Approaches

2.3.1 Equilibrium Methods

The classic means of determining thermochemistry is to measure the equilibrium concentration of reactants and products as a function of temperature and then convert to enthalpies and entropies using the van't Hoff equation. This method can provide the most rigorous thermodynamic determinations and, in the gas phase, can be achieved at both low and high pressures in the presence or absence of buffer gases, but is subject to perturbations associated with sampling the equilibrium zone and uncertainties in the absolute temperature. This method has been used to measure the relative binding energies of alkali cations to a wide range of ligands [32], albeit few biological systems partly because of their limited volatility.

2.3.2 Kinetic Method

The kinetic method was first developed by Cooks and coworkers as a simple method to estimate thermodynamic values from easily performed experiments [33, 34], namely the relative intensities of products resulting from dissociation of a proton (or cation or anion) bound dimer. It has been revised to attempt to include important entropic effects [35, 36], and has been discussed thoroughly [37–39]. Ultimately, it cannot provide true thermodynamic values because the temperature of the evaluation is ill-defined, but does provide useful relative information in the absence of more definitive data.

2.3.3 Blackbody Infrared Radiative Dissociation

Blackbody infrared radiative dissociation (BIRD) allows ions to reach equilibrium with their thermal surroundings by absorption of infrared radiation [40, 41]. Quantitative assessment of the extent of dissociation observed as a function of the temperature of the surroundings allows thermodynamic information to be extracted.

2.3.4 Ion Mobility

In ion mobility studies, ions are dragged through a viscous medium (usually He and more recently N_2) by an electric field [42–44]. The rate at which the ions move in this environment depends on their interaction cross section with the gas, such that larger ions move more slowly than compact ions. Using this technique, the size of ions can be assessed, and by comparison with theoretical structures, the structures of ions can be inferred.

2.4 Theoretical Calculations

Experimental studies of the interactions of alkali metal cations with biological molecules rely on quantum chemistry calculations to provide structural information and molecular parameters useful for interpreting the data. Although some results could be achieved in the absence of theoretical input, the synergy between experiment and theory provides much more robust and detailed results. In this chapter, we focus on theoretical results that provide such synergistic information to experiment, and do not include theoretical results for which there are no complementary experimental data.

Specific computational approaches to alkali metal cation complexes of biomolecules vary nearly as much as the number of investigators that have investigated these systems, but in the laboratories of the authors, the relatively small systems that have been studied have led to an approach that appears to provide accurate

structural and thermodynamic information. For systems where all-electron calculations can be performed, structures and harmonic vibrational frequencies are typically calculated using the hybrid density functional B3LYP coupled with a double or triple zeta basis set, 6-31G(d), 6-31+G(d,p), or 6-311+G(d,p) being common. This is followed by single point energy calculations performed using a larger basis set, 6-311+G(2d,2p), needed to yield accurate energetics, again using B3LYP as well as MP2(full) and sometimes B3P86 or M06 approaches. For calculations of metal-ligand bond dissociation energies (BDEs), basis set superposition error (BSSE) corrections at the full counterpoise level are applied [45, 46]. We generally use multiple computational approaches because different levels of theory often do not agree on the relative energies of low-lying conformations and calculated metal cation-ligand binding energies generally exhibit a spread comparable to experimental uncertainties. These disparate results properly reflect the uncertainties in the computational results.

For the heavier Rb and Cs alkali metal systems, basis sets that utilize effective core potentials (ECPs) are generally used. Extensive testing has demonstrated that even when augmented by additional polarization functions [47], the commonly used LANL2DZ basis set [48] does not provide accurate thermodynamic information [49, 50]. Accurate energetics are provided by using def2-TZVP (or def2-TZVPPD) basis sets, which are balanced basis sets on all atoms at the triple-ζ level including polarization (P) and diffuse (D) functions that use ECPs on rubidium and cesium developed by Leininger et al. [51]. These basis sets are used along with B3LYP for structure and vibrational frequency calculations followed by single point energy calculations using B3LYP, MP2(full), B3P86, or M06 levels.

For the lightest alkali cation, Li^+, we have found that strongly bound ligands are sufficiently close to the 1 s core electrons of the cation that repulsive interactions play a role [52]. Larger basis sets cannot compensate for this repulsion, which requires that the core electrons be permitted to polarize away from the ligand. This can be accomplished using the correlation consistent polarized core/valence basis sets (cc-pCVnZ where n = D, T, and Q) of Woon and Dunning for lithium [53]. For consistency, cc-pVnZ or aug-cc-pVnZ basis sets are used on all other atoms. This approach has been found to yield good thermodynamic values with reasonable computational cost [52]. The def2 and cc-pCVnZ basis sets can be obtained from the Environmental Molecular Sciences Laboratory basis set exchange library [54, 55].

Theory is also used to provide the isotropic molecular polarizabilities of neutral molecules needed for thermochemical analysis of TCID data as well as examination of periodic trends as discussed below. The PBE0/6-311+G(2d,2p) level of theory has been shown to provide polarizabilities that are in good agreement with measured values [56].

As the biological molecules considered increase in size, the methods noted above become increasingly cumbersome largely because a thorough exploration of the enormous conformational space of such molecules becomes expensive. More advanced techniques such as replica exchange molecular dynamics (REMD) [57, 58] or various approximations [59–62] can then be used.

3 Alkali Metal Cations Interacting with Amino Acids

3.1 Structure

Unlike in solution, amino acids in the gas phase are generally not zwitterionic because there is no solvent to support the separated charges. Although alkali cations can yield such zwitterionic structures in a salt-bridge configuration, most alkali metal cation–amino acid complexes, M^+(AA), involve charge solvated structures in which the cation is solvated by the various heteroatoms of the amino acid. For most naturally occurring amino acids and alkali metal cations, the structures of these complexes have been examined in extensive IRMPD spectroscopic studies [63–82]. In the case of proline (and several related molecules), these spectroscopic results have been augmented by structural assignments from TCID studies [83]. In both cases, structures are assigned on the basis of comparison to computational results, IR spectra or BDEs (see next section), respectively.

The results of this work are compiled in Table 1 where it can be seen that the structures evolve as the metal ion changes. For the smallest alkali metal cation, Li^+, the higher charge density leads to tridentate structures in which the metal binds to the

Table 1 Structures of M^+(AA) complexes of alkali metal cations with amino acids.[a]

AA	Li^+	Na^+	K^+	Rb^+	Cs^+
Gly[b]		NO			
Pro[c]	ZW[d]	ZW[b,d]	ZW, OX[e]	ZW, OX	OX, ZW
Ser[f]	NOS	NOS	NOS, OX	NOS, OX	NOS, OX, ZW
Thr[g]	NOS	NOS	NOS, OX	NOS, OX	NOS, OX, ZW
Cys[h]	NOS	NOS	OX, NOS, ZW	OX, NOS, ZW	OX, NOS, ZW
Met[i]	NOS	NOS	NOS, ZW, OX(S)?	NOS, ZW, OX(S)?	NOS, ZW, OX(S)?
Phe[j]	NOS	NOS	NOS[j]	NOS, OS	NOS, OX, OS
Tyr[k]			NOS		
Trp[l]	NOS	NOS, OS	NOS, OS	OS, NOS	OS, NOS
Asp[m]	NOS				OXS, NOS[n]
Glu[m]	NOS				OXS, OS, NOS[n]
Asn[o]	NOS	NOS	NOS, OXS	NOS, OXS	NOS, OXS
Gln[p]	NOS	NOS, OS, OXS?	NOS, OS, OXS?		OXS, OS, NOS
Lys[q]	NOS	NOS	OS, NOS, ZW		
Arg[r]	NOS	ZW, NOS	ZW	ZW	ZW
His[s]	NOS	NOS[t]	OS, NOS, OX	OS, NOS, OX	OS, OX, NOS

[a]Isomers are given in order of approximate relative population, ?=may be present. SC=side-chain heteroatom or aromatic ring, NO=bidentate [N,CO], NOS=tridentate [N,CO,SC], OS=bidentate [CO,SC], OX=bidentate carboxylic acid [COOH], OXS=tridentate carboxylic acid [COOH,SC], ZW=bidentate zwitterion [CO_2^-], OX(S)=OX or OXS or both.
[b][63]. [c][78]. [d][83], TCID. [e][69]. [f][71]. [g][72]. [h][79]. [i][76]. [j][77]. [k][64]. [l][65]. [m][70]. [n][81].[o][75]. [p][73]. [q][68]. [r][66,67]. [s][80]. [t][74].

amino nitrogen and carbonyl oxygen of the backbone along with the heteroatom or aromatic ring of a functionalized side-chain. This gives a tridentate metal ion coordination of [N,CO,SC] as illustrated for the sulfur side-chain of methionine in Figure 1. The single exception is proline, where the unique secondary nitrogen stabilizes a bidentate zwitterionic structure [CO_2^-] in which the metal ion binds to both oxygens of the carboxylate anion, which is hydrogen bonded to the protonated amino group forming a salt-bridge structure. For Na^+, this structural motif is largely maintained although tryptophan and glutamine exhibit bidentate structures that bind only to the backbone carbonyl and the side-chain aromatic ring or carbonyl of the amide group, [CO,SC]. The basic amino acid, arginine, also switches to having predominantly a zwitterionic structure, although the tridentate species is still observed. Glycine, where the cation binds to the amino nitrogen and carbonyl oxygen [N,CO], is also not tridentate, but only because it has no functionalized side-chain.

Because of the lower charge density on the heavier alkali cations, K^+, Rb^+, and Cs^+, these M^+(AA) complexes exhibit several different isomers, with the tridentate [N,CO,SC] structures still present but can be dominated by the bidentate [CO,SC] structures or by bidentate or tridentate structures where the ion binds to the oxygens

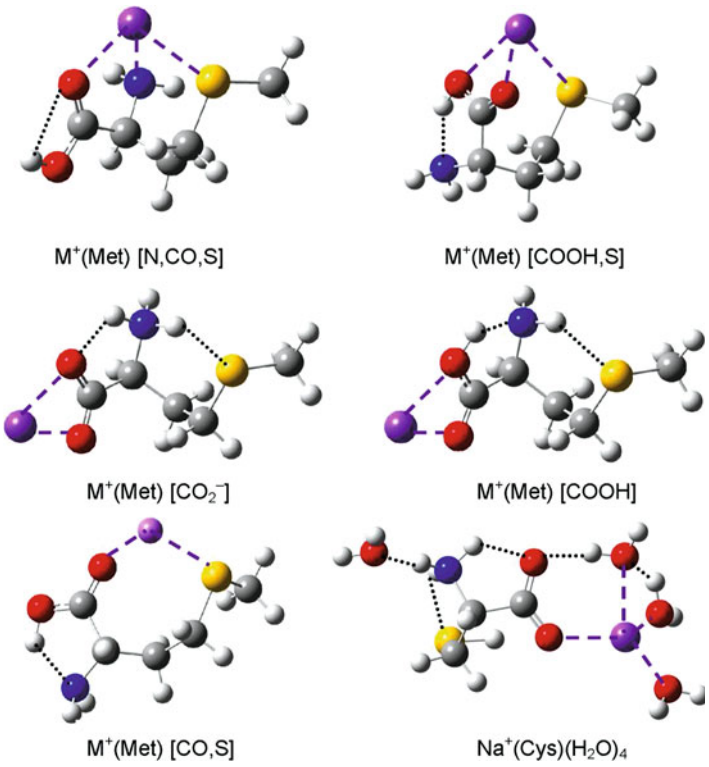

Figure 1 Structures of M^+(Met) and $Na^+(Cys)(H_2O)_4$ showing types of metal coordination (dashed lines). Dotted lines indicate hydrogen bonds.

of the carboxylic acid group, [COOH] and [COOH,SC], respectively, instead of to the amino nitrogen. Even for these metal cations, the only amino acids exhibiting dominant zwitterionic structures are proline and arginine; however, such structures are also observed for Ser, Thr, Cys, and Met. In these cases, the [CO_2^-] structures are accompanied by [COOH] and it can be realized that these two species differ only in whether the proton has transferred to the amino group [CO_2^-] or remains on the oxygen of the carboxylic acid [COOH] (see Figure 1). In both cases, this proton is shared between the backbone amino and carboxyl moieties and the metal cation binds to both carboxyl oxygens, thereby providing the driving force for moving the proton away from the oxygen. As such, these two structures actually lie in a single double-well potential that favors [CO_2^-] when the metal charge density is high (e.g., for metal dications, Li^+ and Na^+) and favors [COOH] when the metal charge density is low (Rb^+ and Cs^+) [71, 80]. Interestingly, computations indicate that the zero point energy of this proton motion generally lies above the bottom of both wells, meaning that the wavefunction associated with the ground vibrational level samples both [COOH] and [CO_2^-] potential wells. This allows simultaneous observation of the CO stretches characteristic of the carboxylate and carboxylic acid groups. Zwitterionic structures are not observed for Li^+ and Na^+ because the [N,CO,SC] structures are strongly favored, whereas the [COOH] (and accompanying [CO_2^-]) structures become competitive for Rb^+ and Cs^+ (and sometimes K^+).

In all of these cases, the structures found are generally in good agreement with computational results of the relative stabilities of the different isomers, although this requires that all accessible conformations are located. For example, assignments for the structure of Cs^+(Glu) were revised after locating a lower energy tridentate [COOH,SC] conformation [70, 81]. In addition, the computed ground isomer can vary substantially with the level of theory used. In many of our own results, we have found that the relative stabilities predicted by single point energy calculations at the MP2 level are preferred compared to B3LYP results. Finally, it has been shown that the conditions used in the source can influence the structures observed, kinetically trapping excited isomers [84].

3.2 Thermodynamics

The evolution of the structures of alkali metal cation-amino acid complexes in the gas-phase as elucidated by IRMPD spectroscopy is fruitfully understood by considering the strength of the interactions with the simplest amino acid, glycine, and molecules representing its various functional components, specifically, 1-propyl amine, 1-propanol, methyl ethyl ketone, propionic acid, and ethanol amine [85, 86]. For Na^+ complexes [85], the molecules having only one functional group bind in the order $OH < NH_2 < CO$. Computations indicate that Na^+ binds to both oxygens of propionic acid, which increases the BDE relative to 1-propanol (by 5 kJ/mol experimentally), but decreases the BDE compared to methyl ethyl ketone (by 13 kJ/mol experimentally). This difference can be attributed to a better orientation of the metal cation in the ketone (which prefers a ∠NaOC bond angle of 180°) coupled with an

inductive effect of the hydroxyl group. Compared with the ketone, glycine binds Na^+ more strongly by 33 kJ/mol, a result of the bidentate binding to both the amino group and the carbonyl, [N,CO]. Interestingly, ethanol amine binds Na^+ more tightly than Gly by 11 kJ/mol because the sp^2 hybridization of the carboxylic acid group of Gly leads to greater conformational restrictions, whereas the sp^3 carbon in ethanol amine provides more flexibility and better overlap of the heteroatom lone pairs and the metal cation.

When a similar analysis is conducted for potassium ion complexes [86], the relative results are similar although the absolute BDEs are 74 ± 4 % of those for Na^+. The most notable difference between the metals lies in the observation that the molecules with single functional groups have BDEs to K^+ in the order $NH_2 < OH < CO$, i.e., the amino group binds less strongly (67 % compared to the Na^+ complex). Because of the poorer binding to the amino group, most levels of theory indicate that K^+(Gly) has a [COOH] ground structure, with [N,CO] (corresponding to the ground conformer for Na^+(Gly)) lying 1 – 7 kJ/mol higher in energy. One driving force for this change is that the larger potassium cation prefers to bind to the ground structure of glycine, which is stabilized by a OH•••N hydrogen bond, whereas the smaller sodium cation binds sufficiently strongly that it preferentially binds to a higher energy conformer of Gly. Results comparable to those of K^+ are expected for the larger alkali metal cations, Rb^+ and Cs^+.

Given these results, the trends in Table 1 are clearer. The alkali metal cations prefer to bind to carbonyl groups, which are always available along the backbone. The smaller cations also like to bind to the amino group and then augment these interactions by binding to the side chain. As the metal cation gets larger, the preference for binding to the amino group in the [N,CO,SC] isomers decreases compared to [COOH,SC] and [COOH] isomers. The larger metal cation also makes it more difficult to maintain strong binding to all three functional groups in the tridentate [N,CO,SC] structure such that the bidentate [CO,SC] structure is competitive.

3.3 Periodic Trends

The interactions of amino acids and alkali metal cations in the gas phase are largely dictated by electrostatics. Table 2 includes a comprehensive listing of the known M^+–AA BDEs measured by TCID [49, 50, 52, 81–83, 85–96], along with a more complete set of values for sodium complexes obtained using the kinetic method [97, 98]. For all AAs, experimental and theoretical results for M^+(AA) BDEs decrease down the periodic table, $Li^+ > Na^+ > K^+ > Rb^+ > Cs^+$. This is primarily a reflection of the increasing radius of the metal cation: 0.70, 0.98, 1.33, 1.49, and 1.69 Å, respectively [99]. The larger cation radius necessarily increases the M^+–AA bond distances, thereby reducing the electrostatic interactions. Experimentally, it is found that BDEs decrease approximately linearly with the inverse of the ionic radius, as shown in Figure 2 for AA = Gly, Pro, and His, with similar plots obtained for other AAs. (Although this inverse dependence seems to suggest a long-range Coulombic potential, the true short-range interactions must comprise combinations of

Table 2 Bond dissociation energies (kJ/mol) at 0 K of M^+(AA) complexes of alkali metal cations with amino acids and small peptides and their polarizabilities (α).[a]

AA	α (Å^3)	Li^+	Na^+	Na^{+b}	K^+	Rb^+	Cs^+
Gly	6.2	220.0 (8.0)[c]	164.0 (4.8)[d]	161 (8)	121.4 (4.8)[e]	108.7 (7.0)[f]	93.3 (2.5)[g]
Ala				167 (8)			
Val				173 (8)			
Leu				175 (8)			
Cys	11.2	255.8 (11.9)[h]	176.9 (5.0)[h]	175 (8)	120.7 (3.1)[h]	102.5 (2.8)[h]	96.8 (4.2)[g]
Ile				176 (8)			
Pro	10.8	254.7 (6.8)[i]	186.2 (4.8)[j]	196 (8)	143.5 (4.5)[j]	125.2 (4.5)[f]	107.9 (4.6)[g]
Asp	10.4		194.9 (5.8)[k]	201 (8)[l]	147.6 (6.8)[m]	126.1 (6.8)[n]	108.9 (6.7)[n]
Glu	12.2		198.8 (4.8)[k]	203 (8)[l]	152.4 (6.8)[m]	134.2 (7.7)[n]	112.6 (6.5)[n]
Ser	8.6	280.8 (12.5)[o]	199.7 (7.7)[o]	192 (8)	144.7 (6.8)[o]	115.7 (4.9)[f]	102.3 (4.1)[g]
Met	14.6	292.0 (12.2)[p]	201.7 (10.6)[p]		141.8 (10.6)[p]	121.0 (7.0)[q]	102.8 (6.6)[q]
Thr	10.5	284.6 (13.5)[o]	203.6 (9.6)[o]	197 (8)	148.6 (9.6)[o]	122.1 (4.6)[f]	105.4 (4.3)[g]
Phe	18.1		205.5 (6.8)[r]	198 (8)	150.5 (5.8)[r]	123.8 (7.2)[q]	112.9 (5.5)[q]
Tyr	18.8		209.4 (9.6)[r]	201 (8)	155.3 (8.7)[r]	125.8 (7.4)[q]	115.6 (6.9)[q]
Asn	11.2		209.4 (5.8)[k]	217 (8)[l]	156.3 (6.8)[m]	138.4 (7.1)[n]	115.3 (6.9)[n]
Gln	13.0		213.2 (5.8)[k]	222 (8)[l]	161.1 (7.7)[m]	144.2 (9.2)[n]	128.1 (8.5)[n]
Trp	22.0		217.1 (7.7)[r]	210 (8)	165.0 (5.8)[r]	138.1 (7.5)[q]	125.0 (6.8)[q]
Lys		<376 (10)[r]	219.0 (10.0)[s]	>213 (8)[l]	155.3 (10.0)[s]	127.4 (8.8)[s]	111.0 (10.0)[s]
His	15.2		222.5 (11.0)[t]	228 (8)[l]	163.5 (8.5)[t]	137.4 (5.7)[t]	118.2 (6.4)[t]
Arg				242 (8)[l]			
Gly_2	11.3		209 (13)[u]	203 (8)[v]	149 (7)[u]		
Gly_3	16.2		240 (17)[u]	237 (9)[v]	183 (15)[u]		
Gly_4	21.1			261 (11)[v]			

[a]Uncertainties in parentheses. [b][97] Kinetic method.
[c][52]. [d][85]. [e][86]. [f][49]. [g][50]. [h][89]. [i][94]. [j][83]. [k][88]. [l][98]. [m][87]. [n][81]. [o][96]. [p][92]. [q][91]. [r][93]. [s][82]. [t][90]. [u][116]. [v][133].

ion-dipole (r^{-2}), ion-quadrupole (r^{-3}), and ion-induced dipole (r^{-4}) forces along with complex chelation effects.) The slopes of the lines shown in Figure 2 for Gly, Pro, and His complexes are 158 ± 6, 190 ± 8, and 214 ± 15 Å kJ/mol, respectively, and properly reflect the relative strength of the interactions of different AAs with the metal cations in that Gly is the weakest binding AA and His is the strongest binding AA measured to date. Direct comparison of the BDEs shows that relative to Na^+(AA) complexes, BDEs for Li^+(AA) are 144 ± 11 %, K^+(AA) are 74 ± 3 %, Rb^+(AA) are 56 ± 21 %, and Cs^+(AA) are 46 ± 21 %.

It can be seen in Figure 2 that the BDEs for Rb^+(His) and Cs^+(His) lie below the linear correlation line, whereas those for Na^+(His) and K^+(His) lie above it, i.e., the larger metal cations show a smaller enhancement in binding associated with the His side chain. Similar effects are also observed for Ser, Thr, Cys, Asp, Glu, and Asn.

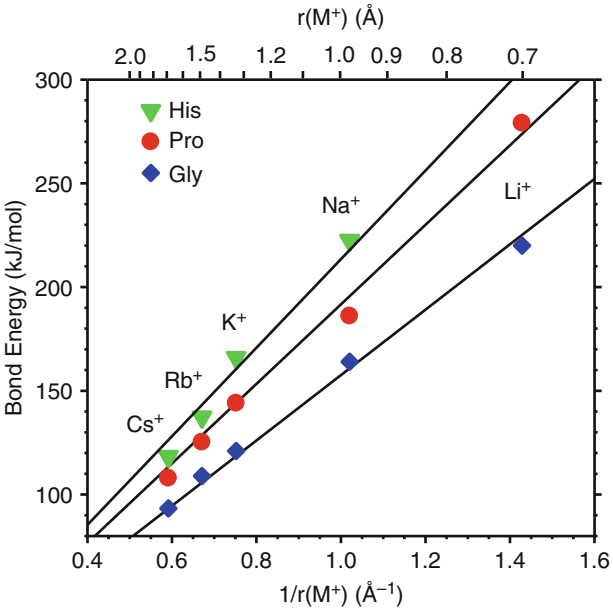

Figure 2 Experimental 0 K bond dissociation energies (in kJ/mol) for M^+(Gly) (blue diamonds), M^+(Pro) (red circles), and M^+(His) (light green triangles) for $M^+ = Li^+$, Na^+, K^+, Rb^+, and Cs^+ are plotted *versus* the inverse metal cation radius (in $Å^{-1}$). The lines are linear regression fits to the data constrained to pass through the origin. Adapted from [90].

These trends can be explored more thoroughly by examining the M^+(AA) BDEs as a function of the polarizability of the AA, as shown in Figure 3 for Na^+ and Cs^+.

Originally, it was found that the BDEs for Gly and the aromatic amino acids (Phe, Tyr, and Trp) exhibited a good correlation with polarizability [93], and this correlation was later extended to include Cys, Met, and Pro [1], as shown in Figure 3 in blue. In both cases, the lines are regression analyses of the data shown. For all alkali metal cations, Asp, Glu (in green), Ser, Thr, Asn, Gln, and His (in red) all exhibit enhanced binding compared to values predicted from the original polarizability correlation [90–92]. For Na^+ (as well as K^+), BDEs to Ser, Thr, Asn, Gln, and His form series that parallel those for the aliphatic AAs. The average enhancement for these five AAs is ~28 and 24 kJ/mol for Na^+ and K^+, respectively [90, 92]. Asp and Glu form a separate series with enhancements of ~15 kJ/mol for both Na^+ and K^+. Compared to Asn and Gln, the carboxylic acid side chains of Asp and Glu bind less tightly because the inductive effect of the hydroxyl group removes electron density from the carbonyl, as noted in Section 3.2 above. It can also be seen that Glu and Gln bind more tightly than Asp and Asn, respectively, because the longer side chain allows more flexibility in the orientation of the side-chain binding. The magnitude of these enhancements has been related to the local dipole moment of the side-chain coordinating site, small for Met, Phe, Tyr, and Trp, relatively large for Ser, Thr, Asn, and Gln, and intermediate for Asp and Glu. Thus,

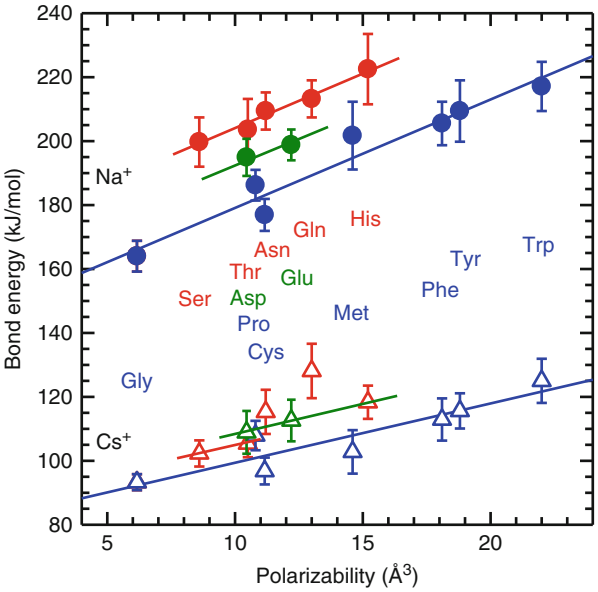

Figure 3 Experimental 0 K bond dissociation energies (in kJ/mol) for Na^+(AA) (circles) and Cs^+(AA) (triangles) versus the calculated polarizability (in Å^3) of the amino acid. The blue lines show linear regression analyses of the data, and the red and green lines are parallel to the regressions. Adapted from [81] and [90].

even though His has a polarizability (15.2 Å^3) comparable to Met (14.6 Å^3), it binds to the alkali cations much more tightly, even exceeding Trp, which has a much higher polarizability (22.0 Å^3). The local dipole moment can be quantified by considering molecules similar to the side chains. Specifically, acetamide (mimicking Asn and Gln) and imidazole (His) have dipole moments of 3.68 and 3.8 D, whereas the 1.70 D dipole moment of acetic acid (Asp and Glu) is about half as large [100]. Methanol (mimicking Ser and Thr) also has a dipole of 1.70 D, which suggests that the side-chain enhancements are influenced by the alignment of the dipole as well as its magnitude. This alignment is influenced by the length of the side-chain, with the two atom lengths (from backbone C_α to coordinating atom) of Ser and Thr being more restrictive than the three atom (Asn, Asp, His) and four atom (Gln, Glu) lengths.

For Cs^+ (as well as Rb^+), the polar side chains of Ser, Thr, Asp, Asn, Glu, Gln, and His also lead to enhanced binding. For Cs^+, Ser and Thr lie ~7 kJ/mol above the trend line [49, 50], Asp, Glu, and His lie ~10 kJ/mol above the trend [90], and Asn and Gln are 15 and 24 kJ/mol higher, respectively. For Rb^+, these same AAs show enhancements of 5 – 7, ~15 kJ/mol, and ~24 and ~24 kJ/mol, respectively. The changes in these side-chain enhancements relative to the smaller cations can be understood in part on the basis of the length of the side chain. For Ser and Thr,

where the side chain is only two atoms long, the enhancement drops from 28 to 24 to 10 to 7 kJ/mol for Na^+ to K^+ to Rb^+ to Cs^+. This decrease is a consequence of the increasing metal cation radius and the fact that larger cations cannot take advantage of binding in a tridentate conformation as well as the smaller cations [49, 50]. Gln has a side-chain length of four atoms and an enhancement that is largely independent of the metal, 24 – 28 kJ/mol, suggesting that the longer side chain allows better tridentate binding for the strongly binding carbonyl group of the carboxamide. For Asp, Glu, and His, with three, four, and three atom side-chain lengths, the enhancements drop from 28 (Na^+) to 24 (K^+) to 15 (Rb^+) and 15 (Cs^+) kJ/mol. This is again consistent with better tridentate binding than the short side chain AAs, but less effective binding than with Gln because the side chain moieties of Asp, Glu, and His do not bind as tightly as the carboxamide. Asn also possesses this carboxamide group but a shorter side-chain than Gln and it shows a trend of 28 (Na^+), 24 (K^+), 24 (Rb^+) and 15 (Cs^+) kJ/mol, intermediate between the strong effect of Gln and the weaker effects of Asp, Glu, and His.

3.4 Effects of Hydration

For several of the sodiated amino acids, Gly, Pro, and Cys, TCID and theoretical studies have examined the effects that hydration exerts on the structure and binding [101–103]. In the gas-phase, hydration effects can be studied for the sequential addition of water molecules, in these cases from one to four. Experimental results (matched by theory) show that the sequential binding energies for losing one water molecule and the amino acid from $Na^+(AA)(H_2O)_x$ decrease monotonically with increasing x. Increasing ligand-ligand repulsion and decreasing effective charge on the sodium cation explain this simple trend.

In the case of $Na^+(Gly)(H_2O)_x$, $x = 1$–4, theory finds that hydration changes the coordination site for Na^+ on glycine from [N,CO] for $x = 0$ and 1 to [CO] coordination where one water molecule bridges to the hydroxyl group for $x = 2 - 4$ [101]. Theory indicates that zwitterionic structures are destabilized by the addition of up to four water molecules because solvation of the Na^+ charge center reduces the ability of the complex to support the charge separation. Interestingly, as additional water molecules are added, zwitterionic structures can become the overall ground structures because solvation of both the Na^+ and $-NH_3^+$ charge centers can occur.

Similar conclusions have been reached in an extensive set of experiments by Williams and coworkers for $M^+(Val)(H_2O)_x$, $x = 1 - 6$ and $M^+ = Li^+$, Na^+, and K^+. These results include kinetic data for all systems [104, 105], hydration energies for $x = 1 - 3$ for Li^+ and $x = 1$ for Na^+ obtained using BIRD [106, 107], and the only spectroscopic results for hydrated alkali metal cationized amino acids [108]. The kinetic results indicate a change in metal cation coordination from [N,CO] to [COOH] at $x = 3$ for Li^+ and $x = 2$ for Na^+. Comparison of the hydration BDEs to related molecules were used to suggest that $Li^+(Val)(H_2O)_3$ has a zwitterionic struc-

ture, however, the more sensitive spectroscopic probe indicates that this complex retains a charge-solvated structure through $x=4$.

For $Na^+(Pro)(H_2O)_x$, $x=1-4$, the addition of a single water molecule again does not change the sodium cation coordination from zwitterionic proline [CO_2^-] [102]. Additional waters keep the zwitterionic proline but change the binding to [CO^-] coordination with one of the water molecules bridging to the second carboxylate oxygen. Theory suggests that the third water added can bind to either cationic site, Na^+ or $-NH_3^+$, with comparable energies. Four waters are sufficient to completely solvate both cationic sites. Similar conclusions were drawn for proline methylated at different positions coordinated to Li^+ and Na^+ and one and two waters in kinetic and BIRD studies [109].

For $Na^+(Cys)(H_2O)_x$, $x=0-2$, theory indicates that the sodium ion binds in the [N,CO,S] tridentate configuration with the waters attaching directly to the sodium ion [103]. Some levels of theory suggest that, similar to Gly and Pro, it is isoenergetic for Na^+ to bind to the carbonyl [CO] with one of the water molecules bridging to the hydroxyl oxygen. The third water can bind to Na^+, $-NH_3^+$, or –OH with equivalent BDEs and at $x=4$, the Na^+ and $-NH_3^+$ groups are completely solvated (Figure 1), in part because there is a strong intramolecular S•••HN hydrogen bond. This effect allows the ground structures of $Na^+(Cys)(H_2O)_4$ and $Na^+(Pro)(H_2O)_4$ to be very similar, i.e., the first hydration shells are complete with four water molecules and the AAs are both zwitterionic. Similar trends are expected for other AAs with functionalized side chains.

BIRD has also been used to examine the first and second hydration energies of Li^+(Gln) and Na^+(Gln) [110, 111] and the first hydration energies of Li^+(Lys) [112]. In all cases, hydration is not found to affect the coordination of these metal cations to the amino acid, which retain charge-solvated structures in all cases. In contrast, IRMPD spectra of $M^+(Arg)(H_2O)$ where $M^+=Li^+$ and Na^+ indicate that the coordination of Li^+ changes from charge-solvated tridentate [N,CO,N] to a zwitterionic [N,CO^-] coordination, whereas Na^+ maintains its zwitterionic [CO_2^-] coordination upon hydration [113]. Kinetic studies indicate that a second water binds to the metal cation, whereas the third likely binds to the cationic guanidinium side chain.

When comparing the hydration energies from system to system, BDEs for losing water from $Na^+(Pro)(H_2O)_x$ are 9–12 kJ/mol smaller at each x compared to $Na^+(Gly)(H_2O)_x$ [102]. This result simply reflects the stronger binding of Na^+ to proline compared to glycine. This inverse correlation has been further substantiated by thermodynamic studies of additional AAs. Using high pressure equilibrium methods, Wincel measured hydration energies for $x=1-3$ of Na^+(AA) where AA = Val, Pro, Met, Phe, and Gln [114] (with good agreement with BIRD results for Val and Gln and reasonable agreement with the TCID studies for Pro). He has also documented a similar trend for hydration of K^+(AA) where AA = Gly, Ala, Val, Met, Pro, and Phe [115].

4 Alkali Metal Cations Interacting with Peptides

4.1 Structure

4.1.1 Di- and Tripeptides

The simplest peptides, di- and triglycine, complexed with sodium cations have been examined using theory and IRMPD spectroscopy [116, 117]. The IRMPD results clearly show that the metal cation coordinates with all carbonyl groups but cannot distinguish whether the N-terminal amine group is also coordinated, in agreement with theory which shows both structures are low-lying. Similar results are obtained for complexes of Li^+ [118], Na^+ [117], K^+ [118–120], and Cs^+ [118] with di- and trialanine. Theory indicates the same is also true for potassiated di- and triglycine [116].

When the peptides are functionalized, the side chain can also participate in the metal coordination. IRMPD results for PheAla and AlaPhe demonstrate that sodium and potassium cations coordinate with the phenyl ring of the side chain (SC) in either a [CO,CO,SC] or [N,CO,SC] geometry [121]. Similar coordination is obtained for the double-π system PhePhe bound to Li^+, Na^+, K^+, and Cs^+ [122], although alkaline earth dications move to an intercalating [CO,CO,SC,SC] coordination. Potassiated HisGly is similar with an apparent [CO,CO,SC] geometry being favored [123]. Comparison of the spectra of potassiated AlaAla, AlaAlaAla, PheAla, PhePhe, and PheGlyGly also reveal extensive similarities with four major peaks near 1750, 1650, 1520, and 1150 cm^{-1} [120]. These correspond to the C-terminal carboxylic carbonyl stretch mediated by metal coordination, the amide I (CO stretch of amide linkages) and amide II (NH bend plus CN stretch, also metal mediated) bands, and the free COH hydroxyl bending mode, respectively.

IRMPD results for GlyArg and ArgGly indicate more profound differences resulting from the sequence inversion [124, 125]. For M^+(GlyArg) where $M^+ = Li^+$, Na^+, and Cs^+, the metal cation coordination is [CO,CO^-] where there is a salt-bridge between the carboxylate anion and protonated guanidine side chain, a geometry favored by a nearly linear arrangement of formal charge sites. In contrast, for M^+(ArgGly) where $M^+ = Li^+$, Na^+, K^+, and Cs^+, the [CO,CO^-] salt-bridge geometry is maintained for the larger cations, whereas Li^+ has a [CO,CO,SC] coordination and Na^+ shows a mixture of this and the salt-bridge structures.

4.1.2 Larger Peptides

The Ohanessian group has systematically examined the structures of Na^+ complexes of polyglycine (Gly_n) for $n = 2 - 8$ using IRMPD [117, 126, 127]. For the smaller peptides, $n = 2 - 5$, all peptidic carbonyls coordinate to the metal cation in globular structures. At $n = 6$, the peptide is sufficiently long that hydrogen bonding interactions between the termini may occur. Larger peptides can no longer tightly chelate the metal cation with all carbonyls, but rather coordinate with six carbonyls and

stabilize the complex by hydrogen bonding interactions, mainly between the termini. Although calculations suggest the zwitterionic structure in which the proton has transferred is low in energy, the experimental spectra support the presence of only the charge solvated structure.

Dunbar et al. used IRMPD to explore the effect of the metal cation identity [128] on the conformations of pentaalanine (Ala_5), finding that Na^+ could bind five carbonyls whereas the larger K^+ and Cs^+ cations prefer structures in which fewer carbonyls coordinate the metal cation allowing the C-terminal carboxyl group to hydrogen bond (as identified by very weak carbonyl bands at 1750 cm^{-1}). This occurs because the weaker binding of these metal cations allows the intramolecular hydrogen bonding to become thermodynamically competitive and influence the coordination.

Larger peptides allow more extensive hydrogen bonding, leading to the familiar helices and sheets in the secondary structures of proteins. However, the conformational space that can be explored for these large peptides is sufficiently large that theoretical calculations are challenging. Nevertheless, IRMPD studies have examined the transition from the globular structures noted above to helices in the case of $Na^+(Ala_n)$ complexes for $n = 8 - 12$ [129] (see Figure 4). The spectrum for the octapeptide indicates that both globular and helical structures contribute, the nonapeptide also has features of both types, and the larger oligopeptides switch to the helical form. Theory indicates the helical form is the lowest in energy for all of these peptides with the globular structures having accessible relative free energies. These results agree with previous ion mobility measurements that demonstrate helical forms for Ala_n where $n = 12 - 20$ complexed with all five alkali cations [130, 131]. Deviations from helicity may occur for smaller peptides (especially lithiated and

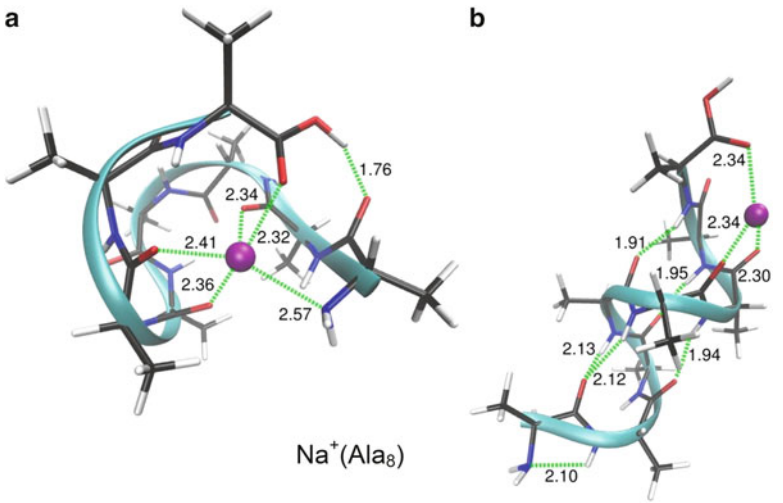

Figure 4 Structures of $Na^+(Ala_8)$ for the lowest energy globular structure (**a**) and α-helical structure (lowest energy, part **b**) as calculated at the M06/6-311+G(d,p)//M06/6-31 G(d,p) level of theory. Bond lengths (Å) for metal coordination and hydrogen bonds are indicated by green dashed lines. Reproduced from [129] with permission from the American Chemical Society; © copyright 2012.

sodiated) where experiments extend down to $n=6$, but the mobility measurements cannot definitively distinguish the two forms.

4.2 Thermodynamics

Thermodynamic studies of metal cations interacting with small peptides are less extensive than for isolated amino acids and IRMPD studies. At this writing, TCID work includes only Na^+ and K^+ bound to glycylglycine (Gly_2) and glycylglycylglycine (Gly_3) [116], which supercedes earlier studies by Klassen et al. [132]. The TCID values for the two sodiated peptides agree nicely with kinetic method results (Table 2), which also examined the sodium cation affinities of tetraglycine (Gly_4) as well as many other di- and tripeptides [133]. These experimental BDEs agree reasonably well with theoretical values [133–137] (see also [116]).

The experimental BDEs for sodiated and potassiated Gly, Gly_2, Gly_3, and Gly_4 increase with the size of the peptide, which can be related to the increasing number of carbonyl groups as well as the increasing polarizability of the peptide (Figure 5). As for any other ligand, the sodium cation affinities are greater than the potassium cation affinities. All levels of theory predict charge-solvated structures for M^+(peptide). As noted above, the metal cations prefer to bind in [CO,CO] bidentate or [N,CO,CO] tridentate configurations in $M^+(Gly_2)$, [CO,CO,CO] tridentate configuration in $M^+(Gly_3)$, and [CO,CO,CO,CO] or [N,CO,CO,CO,CO] structures in $M^+(Gly_4)$. Notably, the increasing BDE with increasing residues begins to level off at Gly_4. This is expected on the basis of decreasing charge density on Na^+ with increasing coordination number and with increased steric constraints [1].

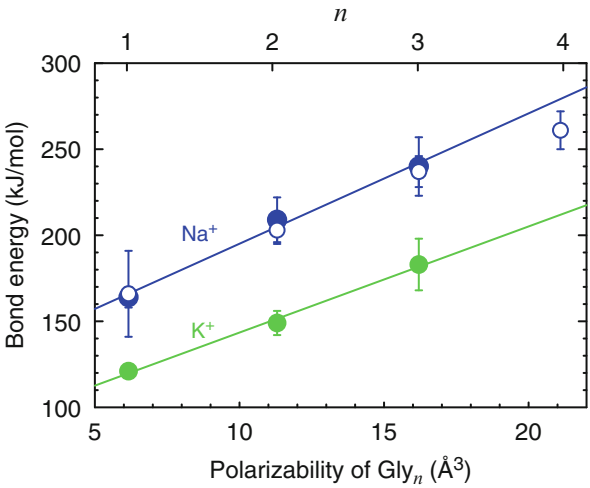

Figure 5 Experimental 0 K BDEs of $M^+(Gly_n)$ versus the theoretical molecular polarizability of Gly_n where n=1–4 and $M^+=Na^+$ and K^+ taken from [116] (solid symbols) and [133] (open symbols). Adapted from [116].

As for the amino acids (Figure 3), the BDEs correlate nicely with the polarizability of these peptides (Figure 4). Notably, this correlation differs from that shown in Figure 3, which can be appreciated by noting that the BDEs of Gly_2 and Asn (isomers of one another and having similar polarizabilities) are similar for both Na^+ and K^+. As for the side-chain enhancements in Figure 3, the local dipole moments of the coordinating carbonyl sites of the peptides must play a role (again consistent with the similarity between Gly_2 and Asn). Although theory does find that the local dipole moments of the peptides are aligned with the metal ion in these complexes [116, 137], there is no direct correlation between the BDEs and calculated dipole moments of Gly, Gly_2, and Gly_3 in their ground complexed geometries (3.2, 5.8, and 5.2 D for Na^+, respectively, and 6.2, 5.9, and 7.8 D for K^+, respectively [116]). Not surprisingly, this indicates the cation affinities of complex species like peptides must involve a superposition of electrostatic and steric effects.

Using the kinetic method, sodium cation binding energies to nineteen peptides containing 2 – 4 residues have been determined and compared favorably to theoretical values [133]. These studies conclude that sodium cation coordination involves all available carbonyls in the most stable structures and that functionalized side chains augment the binding as well. In a comparison of three isomeric pairs of dipeptides (GlyPhe and PheGly, AlaTrp and TrpAla, and GlyHis and HisGly), locating the functionalized side chain at the N-terminus augments the cation affinity more than when it is at the C-terminus by 3 – 12 kJ/mol.

5 Alkali Metal Cations Interacting with Nucleobases

5.1 Structure

Because of the aromaticity of the heterocyclic rings of the nucleobases, there is much less conformational flexibility compared to the amino acids. Theoretical studies indicate that metal cation-nucleobase complexes are nearly planar, with π-bound complexes lying considerably higher in energy. For adenine (A), IRMPD spectroscopy near 3500 cm^{-1} indicates that Li^+, Na^+, K^+, and Cs^+ all bind to A at the N3 and N9 positions [138] (see Figure 6 for the nomenclature used). This tautomer, which differs from the canonical form shown in Figure 6 by moving the H9 hydrogen to N7, is less relevant biologically because the sugar attaches to N9 in nucleosides and nucleotides. Addition of a single water left this binding mode unchanged. In the case of cytosine (C), IRMPD spectroscopy of complexes with all five alkali metal cations yield similar spectra, although the Rb^+ and Cs^+ complexes are richer in spectral details [139]. Although small changes in the positions and shape of the bands are observed to correlate with the size of the metal cation, all five spectra can be explained by a single isomer in which the cation binds to the O2 and N3 atoms of the canonical cytosine structure shown in Figure 6, in agreement with computations.

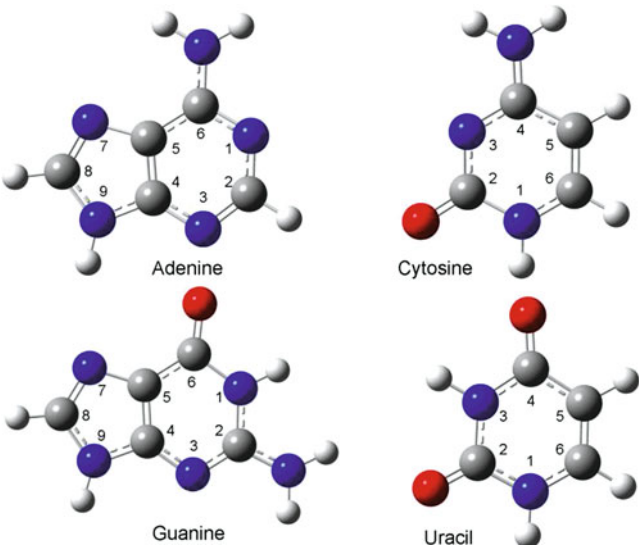

Figure 6 Structures of adenine, cytosine, guanine, and uracil.

In the case of uracil (U), IRMPD spectroscopy unambiguously shows that Li^+ and Na^+ bind at the O4 carbonyl [140, 141]. For thymine (T = 5-methyluracil = m^5U), addition of water, or addition of another base (U or T) to the lithiated complex leaves this binding motif unchanged. If sulfur is substituted at the 2 position (S^2U) without or with methyl substitutions at the 5 and 6 positions (m^5S^2U and m^6S^2U), this binding mode is also retained. In contrast, substitution at the 4 position (in both S^4U and $S^{24}{}_2U$) induces tautomization in which the N3 hydrogen moves to S4 and Na^+ binds at the O2N3 (or S2N3) positions. Likewise, the sodium cation complexes of 5-halogenated uracil retain the O4 binding site for all four halogens (F, Cl, Br, and I), with chelation to the halogen substituent providing additional stabilization [142]. In contrast, $Na^+(cl^6U)$ is found to have multiple isomers present, although the O4 binding site remains a major contributor. For both the U and C studies, various tautomeric structures were also carefully considered in these studies, however, the binding sites observed are biologically relevant because the sugar in nucleosides and nucleotides binds at N1 of uracil and cytosine.

For larger complexes, the number of studies is limited. The effect of sodiation on the conformers of all possible dinucleotides (single-strands, duplexes, and triplexes) was examined using ion mobility [143]. Three types of structural motifs were found: base stacking, perpendicular bases, or coplanar bases with small barriers (4 – 8 kJ/mol) between them. Duplexes and triplexes showed considerably less structural diversity than the single-strand complexes with only one conformer observed for all duplexes except dTG, dGT, and dTT and for all triplexes (where dTG, dGT, and dTT are the DNA dinucleotides possessing T and G = guanine nucleobase residues).

5.2 Thermodynamics

Early TCID studies of M^+(nucleobase) where $M^+ = Li^+$, Na^+, and K^+ and nucleobase = U, T, and A determined the metal cation binding energies for all nine systems [144] (Table 3), which agree reasonably well with theory and also with prior kinetic method results [145] except for Na^+(A). The latter work also includes guanine (G) (Table 3). Subsequent TCID work has extended this work to nucleobase = C [146], where the value for Na^+(C) is again in agreement with kinetic method results [147]. This study also includes the first (and as yet only) extension to Rb^+ and Cs^+ complexes, finding bond energies of 148.0 ± 3.6 and 137.2 ± 4.3 kJ/mol, respectively.

As for amino acids and peptides, the BDEs decrease as the metal cation gets larger. Comparison of experimental BDEs with theoretical results (along with the IRMPD results noted above for U and C) show that the metal cations bind preferentially at the N7 site coupled with chelation to the amino group for A, at the O2 carbonyl and N3

Table 3 Bond dissociation energies (kJ/mol) at 0 K of alkali metal cations with nucleic acid bases and their sites of attachment (SA).[a]

Nucleobase	SA	Li^+	Na^+	K^+
A[b]	$N7NH_2$	226.1 (6.1)	139.6 (4.2)	95.1 (3.2)
C	O2N3[c]		209.5 (5.0)	161.5 (4.5)
	N1O2[d]	235.2 (7.0)	177.6 (5.4)	
G[e]	O6N7	239 (8)	182 (8)	117 (8)
U[b]	O4	211.5 (6.1)	134.6 (3.4)	104.3 (2.8)
m^1U[f]	O4	234.0 (7.2)	150.7 (4.1)	110.9 (2.7)
m^3U[f]	O4	220.9 (6.7)	143.6 (3.8)	107.5 (3.3)
m^5U (= T)[b]	O4	210.1 (7.0)	135.3 (3.8)	104.0 (3.8)
m^6U[f]	O4	222.3 (6.6)	136.6 (5.8)	108.8 (5.4)
$m^{13}{}_2U$[f]	O4	239.8 (7.8)	153.6 (4.7)	118.9 (3.3)
$m^{56}{}_2U$[f]	O4	233.8 (6.5)	136.8 (5.1)	113.2 (3.2)
fl^5U[g]	O4F5	198.9 (4.8)	149.0 (4.3)	110.2 (3.8)
cl^5U[g]	O4Cl5	242.9 (8.2)	141.4 (3.4)	104.1 (2.7)
cl^6U[g]	O4	229.6 (7.8)	139.5 (4.4)	97.8 (2.2)
br^5U[g]	O4Br5	235.9 (5.3)	142.3 (4.8)	109.8 (2.3)
io^5U[g]	O4I5		147.5 (5.7)	117.6 (4.7)
S^2U[h]	O4	216.2 (5.7)	139.8 (3.3)	103.2 (2.6)
m^5S^2U[h]	O4	213.3 (5.5)	142.3 (5.5)	101.2 (2.8)
m^6S^2U[h]	O4	222.0 (6.2)	143.6 (3.8)	106.6 (3.5)
S^4U[h]	O2	213.1 (5.0)	125.8 (4.7)	97.3 (5.5)
$S^{24}{}_2U$[h]	S4	175.1 (4.5)	100.2 (5.8)	80.8 (2.8)[i]

[a]Uncertainties in parentheses. A = adenine, C = cytosine, G = guanine, U = uracil, m = methyl, fl = fluorine, cl = chlorine, br = bromine, io = iodine, S = sulfur. Superscripts indicate the position of the substitution.

[b][144]. [c][146]. [d][149]. [e][145] kinetic method. [f][151]. [g][152]. [h][153].

site of C, at the O6 carbonyl and N7 site of G, and at the O4 carbonyl of U and T. Note that the assignment for A differs from that from the IRMPD work [138], which can be attributed to the different ion sources used to produce the metalized nucleobase. (Interestingly, as originally suggested on the basis of theoretical work [148], earlier TCID [149] and kinetic method work [147] using different ion source methodology appears to have measured thermochemistry for excited isomers of the cytosine complexes, in which the metal cations bind at the N1O2 position, which requires tautomerization from the lowest energy isomer shown in Figure 6. Because the sugar attaches at N1, this isomer is less relevant to biological systems.)

The bidentating binding of C provides the strongest metal cation BDEs. G is also bidentate, but the geometry of the binding sites requires longer metal ligand bonds. A is also bidentate but requires rotation of the amino group in order to chelate and this is energetically costly because of the loss of π-resonance energy. The monodentate M^+(U) and M^+(T) complexes are the weakest binders for Li^+ and Na^+, whereas K^+ binds A most weakly. Notably, these interactions are sufficiently large to potentially disrupt hydrogen bonding in A::T (A::U) nucleic acid base pairs.

A number of studies have examined the effects of modification on these BDEs. Such modified nucleobases are relatively prominent in transfer RNAs, with methylation being most common [150], and can exhibit both therapeutic and harmful effects. The kinetic method has been used to show that Na^+ binds 1- and 5-methyl cytosine more tightly than unsubstituted cytosine by 10 and 5 kJ/mol, respectively [147]. A more extensive series of studies on modified uracils have been conducted using the TCID approach. Methylation at the 5, 6, and 5 and 6 positions has a relatively small effect on the BDEs with Li^+, Na^+, and K^+ (Table 3), whereas methylation at N3 increases the BDE by 5 ± 2 %, at N1 (where the sugar attaches) by 10 ± 2 %, and at both sites by 14 ± 1 % [151]. In contrast, halogenation at the 5 position increases the alkali metal cation BDEs, in part because the halogen can also chelate with the metal [152]. Halogenation at the 6 position, where it can no longer chelate, introduces a much smaller effect (actually decreasing the BDE for K^+). Notably, because halogenation is found to decrease the proton affinity of U, such substitutions should stabilize A::U base pairs, which may provide some insight into their use as antitumor and antiviral agents. Thioketo substitution at the 2 position slightly increases the metal cation BDEs, whereas 4-thioketo U decreases the BDE, especially if both positions are exchanged for sulfur [153]. The latter substitution is predicted to have a marked effect at destabilizing A::SU base pairs.

The thermodynamics of hydration of sodiated and potassiated complexes of A, C, U, and T by one and two waters have also been measured using equilibrium methods [154]. In concert with the results above, these results suggest that tautomerization of cytosine is important in determining the distribution of complexes formed by electrospray ionization. In the case of thiouracils, substitution at the 2 or 4 position has little effect on the first and second hydration energy of the sodiated complexes [155]. Results appear to be consistent with direct binding of water to the sodium cation without disruption of the alkali metal cation-nucleobase structures noted above.

6 Concluding Remarks and Future Directions

Gas-phase studies in combination with computational work are capable of providing considerable detail information regarding how alkali metal cations interact with biological systems ranging in size from simple model compounds through the constituents of proteins and nucleic acids up to peptides and nucleotides. The strength of these approaches are the quantitative structural and thermodynamic information that is afforded. Their weakness is the considerable projection that is needed to apply these data to real biological systems.

However, the exploration of such larger complexes is a very active area of research that promises to bridge the gap between the small molecule chemistry reviewed here and real systems. Such studies will not only directly yield more quantitative information about how secondary structure influences their properties and function, but should allow the lessons learned from small molecules to translate more effectively to the large complex systems.

Abbreviations and Definitions

A	adenine
AA	amino acid
Arg	arginine
Asn	asparagine
Asp	aspartic acid
BDE	bond dissociation energy
BIRD	blackbody infrared radiative dissociation
BSSE	basis set superposition error
C	cytosine
CA	collisional activation
CAD	collision activated dissociation
CID	collision-induced dissociation
CLIO	Centre Laser Infrarouge d'Orsay
Cys	cysteine
dGT	2'-deoxy-guanine-thymine dinucleotide
dTG	2'-deoxy-thymine-guanine dinucleotide
dTT	2'-deoxy-thymine dinucleotide
ECP	effective core potential
EMSL	Environmental Molecular Sciences Laboratory
FEL	free electron laser
FELICE	Free Electron Laser for IntraCavity Experiments
FELIX	Free Electron Lasers for Infrared eXperiments
G	guanine
GIBMS	guided ion beam tandem mass spectrometer

Gln	glutamine
Glu	glutamic acid
Gly	glycine
His	histidine
IR	infrared
IRMPD	infrared multiple photon dissociation
IRPD	infrared photodissociation
IVR	intramolecular vibrational redistribution
Lys	lysine
Met	methionine
MS	mass spectrometer or mass spectrometry
Phe	phenylalanine
Pro	proline
QQQ	triple quadrupole mass spectrometer
REMD	replica exchange molecular dynamics
SC	side chain
Ser	serine
T	thymine
TCID	threshold collision-induced dissociation
Thr	threonine
Trp	tryptophan
Tyr	tyrosine
U	uracil

Acknowledgment We would like to thank the many students that contributed to this work for their dedication, insight, and hard work. The research discussed in this chapter has been supported by the National Science Foundation, Grants No. CHE-1409420 (MTR), CHE-1359769 (PBA), and OISE-0730072.

References

1. M. T. Rodgers, P. B. Armentrout, *Acc. Chem. Res.* **2004**, *37*, 989–998.
2. K. K. Lehmann, G. Scoles, B. H. Pate, *Annu. Rev. Phys. Chem.* **1994**, *45*, 241–274.
3. A. Beil, D. Luckhaus, M. Quack, J. Stohner, *Ber. Bunsen Phys. Chem.* **1997**, *101*, 311–328.
4. J. G. Black, E. Yablonovitch, N. Bloembergen, S. Mukamel, *Phys. Rev. Lett.* **1977**, *38*, 1131–1134.
5. E. Grant, P. Schulz, A. S. Sudbo, Y. Shen, Y. T. Lee, *Phys. Rev. Lett.* **1978**, *40*, 115–118.
6. V. J. F. Lapoutre, B. Redlich, A. F. G. van der Meer, J. Oomens, J. M. Bakker, A. Sweeney, A. Mookherjee, P. B. Armentrout, *J. Phys Chem. A* **2013**, *117*, 4115–4126.
7. A. B. McCoy, X. Huang, S. Carter, M. Y. Landeweer, J. M. Bowman, *J. Chem. Phys.* **2005**, *122*, 061101.
8. C. M. Leavitt, A. F. DeBlase, C. J. Johnson, M. van Stipdonk, A. B. McCoy, M. A. Johnson, *J. Phys. Chem. Lett.* **2013**, *4*, 3450–3457.
9. X. Cheng, R. P. Steele, *J. Chem. Phys.* **2014**, *141*, 104–105.
10. P. B. Armentrout, *J. Am. Soc. Mass Spectrom.* **2002**, *13*, 419–434.
11. K. M. Ervin, P. B. Armentrout, *J. Chem. Phys.* **1985**, *83*, 166–189.

12. D. A. Hales, L. Lian, P. B. Armentrout, *Int. J. Mass Spectrom. Ion Processes* **1990**, *102*, 269–301.
13. R. H. Schultz, K. C. Crellin, P. B. Armentrout, *J. Am. Chem. Soc.* **1991**, *113*, 8590–8601.
14. M. T. Rodgers, K. M. Ervin, P. B. Armentrout, *J. Chem. Phys.* **1997**, *106*, 4499–4508.
15. M. T. Rodgers, P. B. Armentrout, *J. Chem. Phys.* **1998**, *109*, 1787–1800.
16. P. B. Armentrout, *J. Chem. Phys.* **2007**, *126*, 234302.
17. P. B. Armentrout, K. M. Ervin, M. T. Rodgers, *J. Phys. Chem. A* **2008**, *112*, 10071–10085.
18. N. F. Dalleska, K. Honma, P. B. Armentrout, *J. Am. Chem. Soc.* **1993**, *115*, 12125–12131.
19. N. F. Dalleska, K. Honma, L. S. Sunderlin, P. B. Armentrout, *J. Am. Chem. Soc.* **1994**, *116*, 3519–3528.
20. N. F. Dalleska, B. L. Tjelta, P. B. Armentrout, *J. Phys. Chem* **1994**, *98*, 4191–4195.
21. M. T. Rodgers, P. B. Armentrout, *J. Phys. Chem. A* **1997**, *101*, 1238–1249.
22. M. T. Rodgers, P. B. Armentrout, *J. Phys. Chem. A* **1997**, *101*, 2614–2625.
23. C. Iceman, P. B. Armentrout, *Int. J. Mass Spectrom.* **2003**, *222*, 329–349.
24. J. C. Amicangelo, P. B. Armentrout, *J. Phys. Chem. A* **2004**, *108*, 10698–10713.
25. A. L. Heaton, P. B. Armentrout, *J. Am. Chem. Soc.* **2008**, *130*, 10227–10232.
26. A. L. Heaton, S. J. Ye, P. B. Armentrout, *J. Phys. Chem. A* **2008**, *112*, 3328–3338.
27. S. J. Ye, P. B. Armentrout, *J. Phys. Chem. B* **2008**, *112*, 10303–10313.
28. P. B. Armentrout, A. L. Heaton, *J. Am. Soc. Mass Spectrom.* **2012**, *23*, 632–643.
29. P. B. Armentrout, A. A. Clark, *Int. J. Mass Spectrom.* **2012**, *316–318*, 182–191.
30. P. B. Armentrout, E. M. S. Stennett, *J. Am. Soc. Mass Spectrom.* **2014**, *25*, 512–523.
31. U. H. Verkerk, C.-K. Siu, J. D. Steill, H. El Aribi, J. Zhao, C. F. Rodriguez, J. Oomens, A. C. Hopkinson, K. W. M. Siu, *J. Phys. Chem. Lett.* **2010**, *1*, 868–872.
32. P. Kebarle, in *Encyclopedia of Mass Spectrometry*, Ed. P. B. Armentrout, Elsevier, Amsterdam, 2003, Vol. 1, pp. 319–338.
33. S. A. McLuckey, D. Cameron, R. G. Cooks, *J. Am. Chem. Soc.* **1981**, *103*, 1313–1317.
34. R. G. Cooks, P. H. Wong, *Acc. Chem. Res.* **1998**, *31*, 379–386.
35. X. Cheng, Z. Wu, C. Fenselau, *J. Am. Chem. Soc.* **1993**, *115*, 4844–4848.
36. P. B. Armentrout, *J. Am. Soc. Mass Spectrom.* **2000**, *11*, 371–379.
37. P. B. Armentrout, *J. Mass Spectrom.* **1999**, *34*, 74–78.
38. L. Drahos, K. Vekey, *J. Mass Spectrom.* **1999**, *34*, 79–84.
39. R. G. Cooks, J. T. Koskinen, P. D. Thomas, *J. Mass Spectrom.* **1999**, *34*, 85–92.
40. W. D. Price, P. D. Schnier, E. R. Williams, *Anal. Chem.* **1996**, *68*, 859–866.
41. R. C. Dunbar, T. B. McMahon, D. Thoelmann, D. S. Tonner, D. R. Salahub, D. Wei, *J. Am. Chem. Soc.* **1995**, *117*, 12819–12825.
42. S. Lee, T. Wyttenbach, M. T. Bowers, *Int. J. Mass Spectrom.* **1997**, *167/168*, 605–614.
43. C. S. Hoaglund, S. J. Valentine, D. E. Clemmer, *Anal. Chem.* **1997**, *69*, 4156–4161.
44. A. B. Kanu, P. Dwivedi, M. Tam, L. Matz, H. H. Hill, *J. Mass Spectrom.* **2008**, *43*, 1–22.
45. S. F. Boys, R. Bernardi, *Mol. Phys.* **1970**, *19*, 553–566.
46. F. B. van Duijneveldt, J. G. C. M. van Duijneveldt-van de Rijdt, J. H. van Lenthe, *Chem. Rev.* **1994**, *94*, 1873–1885.
47. E. D. Glendening, D. Feller, M. A. Thompson, *J. Am. Chem. Soc.* **1994**, *116*, 10657–10669.
48. P. J. Hay, W. R. Wadt, *J. Chem. Phys.* **1985**, *82*, 284–298.
49. V. N. Bowman, A. L. Heaton, P. B. Armentrout, *J. Phys. Chem. B* **2010**, *114*, 4107–4114.
50. P. B. Armentrout, Y. Chen, M. T. Rodgers, *J. Phys. Chem. A* **2012**, *116*, 3989–3999.
51. T. Leininger, A. Nicklass, W. Kuechle, H. Stoll, M. Dolg, A. Bergner, *Chem. Phys. Lett.* **1996**, *255*, 274–280.
52. M. T. Rodgers, P. B. Armentrout, *Int. J. Mass Spectrom.* **2007**, *267*, 167–182.
53. D. E. Woon, T. H. Dunning, Jr., *J. Chem. Phys.* **1995**, *103*, 4572–4585.
54. K. L. Schuchardt, B. T. Didier, T. Elsethagen, L. Sun, V. Gurumoorthi, J. Chase, J. Li, T. L. Windus, *J. Chem. Inf. Model.* **2007**, *47*, 1045–1052.
55. D. Feller, *J. Comput. Chem.* **1996**, *17*, 1571–1586.

56. S. M. Smith, A. N. Markevitch, D. A. Romanor, X. Li, R. J. Levis, H. B. Schlegel, *J. Phys. Chem. A* **2000**, *108*, 11063–11072.
57. D. Semrouni, C. Clavaguera, J. P. Dognon, G. Ohanessian, *Int. J. Mass Spectrom.* **2010**, *297*, 152–161.
58. N. V. Buchete, G. Hummer, *Phys. Rev. E* **2008**, *77*, 030902.
59. C. Bleiholder, T. Wyttenbach, M. T. Bowers, *Int. J. Mass Spectrom.* **2011**, *308*, 1–10.
60. T. Wyttenbach, G. v. Helden, J. J. Batka, D. Carlat, M. T. Bowers, *J. Am. Soc. Mass Spectrom.* **1997**, *8*, 275–282.
61. M. F. Mesleh, J. M. Hunter, A. A. Shvartsburg, G. C. Schatz, M. F. Jarrold, *J. Phys. Chem. A* **1996**, *100*, 16082–16086.
62. A. A. Shvartsburg, M. F. Jarrold, *Chem. Phys. Lett.* **1996**, *261*, 86–91.
63. C. Kapota, J. Lemaire, P. Maitre, G. Ohanessian, *J. Am. Chem. Soc.* **2004**, *126*, 1836–1842.
64. N. C. Polfer, B. Paizs, L. C. Snoek, I. Compagnon, S. Suhai, G. Meijer, G. von Helden, J. Oomens, *J. Am. Chem. Soc.* **2005**, *127*, 8571–8579.
65. N. C. Polfer, J. Oomens, R. C. Dunbar, *Phys. Chem. Chem. Phys.* **2006**, *8*, 2744–2751.
66. M. F. Bush, J. T. O'Brien, J. S. Prell, R. J. Saykally, E. R. Williams, *J. Am. Chem. Soc.* **2007**, *129*, 1612–1622.
67. M. W. Forbes, M. F. Bush, N. C. Polfer, J. Oomens, R. C. Dunbar, E. R. Williams, R. A. Jockusch, *J. Phys. Chem. A* **2007**, *111*, 11759–11770.
68. M. F. Bush, M. W. Forbes, R. A. Jockusch, J. Oomens, N. C. Polfer, R. J. Saykally, E. R. Williams, *J. Phys. Chem. A* **2007**, *111*, 7753–7760.
69. M. K. Drayss, D. Blunk, J. Oomens, M. Schäfer, *J. Phys Chem. A* **2008**, *112*, 11972–11974.
70. J. T. O'Brien, J. S. Prell, J. D. Steill, J. Oomens, E. R. Williams, *J. Phys. Chem. A* **2008**, *112*, 10823–10830.
71. P. B. Armentrout, M. T. Rodgers, J. Oomens, J. D. Steill, *J. Phys. Chem. A* **2008**, *112*, 2248–2257.
72. M. T. Rodgers, P. B. Armentrout, J. Oomens, J. D. Steill, *J. Phys. Chem. A* **2008**, *112*, 2258–2267.
73. M. F. Bush, J. Oomens, R. J. Saykally, E. R. Williams, *J. Phys. Chem. A* **2008**, *112*, 8578–8584.
74. R. C. Dunbar, A. C. Hopkinson, J. Oomens, C.-K. Siu, K. W. M. Siu, J. D. Steill, U. H. Verkerk, J. Zhao, *J. Phys. Chem. B* **2009**, *113*, 10403–10408.
75. A. L. Heaton, V. N. Bowman, J. Oomens, J. D. Steill, P. B. Armentrout, *J. Phys. Chem. A* **2009**, *113*, 5519–5530.
76. D. R. Carl, T. E. Cooper, J. Oomens, J. D. Steill, P. B. Armentrout, *Phys. Chem. Chem. Phys.* **2010**, *12*, 3384–3398.
77. R. C. Dunbar, J. D. Steill, J. Oomens, *Phys. Chem. Chem. Phys.* **2010**, *12*, 13383–13393.
78. M. K. Drayss, P. B. Armentrout, J. Oomens, M. Schäfer, *Int. J. Mass Spectrom.* **2010**, *297*, 18–27.
79. M. Citir, E. M. S. Stennett, J. Oomens, J. D. Steill, M. T. Rodgers, P. B. Armentrout, *Int. J. Mass Spectrom.* **2010**, *297*, 9–17.
80. M. Citir, C. S. Hinton, J. Oomens, J. D. Steill, P. B. Armentrout, *J. Phys. Chem. A* **2012**, *116*, 1532–1541.
81. P. B. Armentrout, B. Yang, M. T. Rodgers, *J. Phys. Chem. B* **2014**, *118*, 4300–4314.
82. A. A. Clark, B. Yang, R. R. Wu, M. T. Rodgers, P. B. Armentrout, work in progress.
83. R. M. Moision, P. B. Armentrout, *J. Phys. Chem. A* **2006**, *110*, 3933–3946.
84. N. C. Polfer, R. C. Dunbar, J. Oomens, *J. Am. Soc. Mass Spectrom.* **2007**, *18*, 512–516.
85. R. M. Moision, P. B. Armentrout, *J. Phys. Chem. A* **2002**, *106*, 10350–10362.
86. R. M. Moision, P. B. Armentrout, *Phys. Chem. Chem. Phys.* **2004**, *6*, 2588–2599.
87. A. L. Heaton, P. B. Armentrout, *J. Phys. Chem. B* **2008**, *112*, 12056–12065.
88. A. L. Heaton, R. M. Moision, P. B. Armentrout, *J. Phys. Chem. A* **2008**, *112*, 3319–3327.
89. P. B. Armentrout, E. I. Armentrout, A. A. Clark, T. E. Cooper, E. M. S. Stennett, D. R. Carl, *J. Phys. Chem. B* **2010**, *114*, 3927–3937.

90. P. B. Armentrout, M. Citir, Y. Chen, M. T. Rodgers, *J. Phys. Chem. A* **2012**, *116*, 11823–11832.
91. P. B. Armentrout, B. Yang, M. T. Rodgers, *J. Phys. Chem. A* **2013**, *117*, 3771–3781.
92. P. B. Armentrout, A. Gabriel, R. M. Moision, *Int. J. Mass Spectrom.* **2009**, *283*, 56–68.
93. C. Ruan, M. T. Rodgers, *J. Am. Chem. Soc.* **2004**, *126*, 14600–14610.
94. A. Mookherjee, P. B. Armentrout, *Int. J. Mass Spectrom.* **2014**, *370*, 16–28.
95. A. Mookherjee, P. B. Armentrout, *Int. J. Mass Spectrom.* **2013**, *345–347*, 109–119.
96. S. J. Ye, A. A. Clark, P. B. Armentrout, *J. Phys. Chem. B* **2008**, *112*, 10291–10302.
97. M. M. Kish, G. Ohanessian, C. Wesdemiotis, *Int. J. Mass Spectrom.* **2003**, *227*, 509–524.
98. P. Wang, G. Ohanessian, C. Wesdemiotis, *Int. J. Mass Spectrom.* **2008**, *269*, 34–45.
99. R. G. Wilson, G. R. Brewer, *Ion Beams with Applications to Ion Implantation*, Wiley, New York, 1973.
100. *CRC Handbook of Chemistry and Physics*, Ed D. R. Lide, CRC Press, Boca Raton, 2002.
101. S. J. Ye, R. M. Moision, P. B. Armentrout, *Int. J. Mass Spectrom.* **2005**, *240*, 233–248.
102. S. J. Ye, R. M. Moision, P. B. Armentrout, *Int. J. Mass Spectrom.* **2006**, *253*, 288–304.
103. S. J. Ye, P. B. Armentrout, *Phys. Chem. Chem. Phys.* **2010**, *12*, 13419–13433.
104. R. A. Jockusch, A. S. Lemoff, E. R. Williams, *J. Phys. Chem. A* **2001**, *105*, 10929–10942.
105. R. A. Jockusch, A. S. Lemoff, E. R. Williams, *J. Am. Chem. Soc.* **2001**, *123*, 12255–12265.
106. A. S. Lemoff, M. F. Bush, E. R. Williams, *J. Am. Chem. Soc.* **2003**, *125*, 13576–13584.
107. A. S. Lemoff, E. R. Williams, *J. Am. Soc. Mass Spectrom.* **2004**, *15*, 1014–1024.
108. A. Kamariotis, O. V. Boyarkin, S. R. Mercier, R. D. Beck, M. F. Bush, E. R. Williams, T. R. Rizzo, *J. Am. Chem. Soc.* **2006**, *128*, 905–916.
109. A. S. Lemoff, M. F. Bush, E. R. Williams, *J. Phys. Chem. A* **2005**, *109*, 1903–1910.
110. A. S. Lemoff, M. F. Bush, C.-C. Wu, E. R. Williams, *J. Am. Chem. Soc.* **2005**, *127*, 10276–10286.
111. A. S. Lemoff, C.-C. Wu, M. F. Bush, E. R. Williams, *J. Phys. Chem. A* **2006**, *110*, 3662–3669.
112. A. S. Lemoff, M. F. Bush, J. T. O'Brien, E. R. Williams, *J. Phys. Chem. A* **2006**, *110*, 8433–8442.
113. M. F. Bush, J. S. Prell, R. J. Saykally, E. R. Williams, *J. Am. Chem. Soc.* **2007**, *129*, 13544–13553.
114. H. Wincel, *J. Phys. Chem. A* **2007**, *111*, 5784–5791.
115. H. Wincel, *J. Am. Soc. Mass Spectrom.* **2007**, *18*, 2083–2089.
116. S. J. Ye, P. B. Armentrout, *J. Phys. Chem. A* **2008**, *112*, 3587–3596.
117. O. P. Balaj, C. Kapota, J. Lemaire, G. Ohanessian, *Int. J. Mass Spectrom.* **2008**, *269*, 196–209.
118. R. C. Dunbar, J. D. Steill, J. Oomens, *Int. J. Mass Spectrom.* **2010**, *297*, 107–115.
119. R. C. Dunbar, J. Steill, N. C. Polfer, J. Oomens, *J. Phys. Chem. B* **2009**, *113*, 10552–10554.
120. R. C. Dunbar, N. C. Polfer, G. Berden, J. Oomens, *Int. J. Mass Spectrom.* **2012**, *330–332*, 71–77.
121. N. C. Polfer, J. Oomens, R. C. Dunbar, *ChemPhysChem* **2008**, *9*, 579–589.
122. R. C. Dunbar, J. D. Steill, J. Oomens, *J. Am. Chem. Soc.* **2011**, *133*, 9376–9386.
123. R. C. Dunbar, J. Oomens, G. Berden, J. K. C. Lau, U. H. Verkerk, A. C. Hopkinson, K. W. M. Siu, *J. Phys. Chem. A* **2013**, *117*, 5335–5343.
124. J. S. Prell, M. Demireva, J. Oomens, E. R. Williams, *J. Am. Chem. Soc.* **2009**, *131*, 1232–1242.
125. J. S. Prell, T. M. Chang, J. A. Biles, G. Berden, J. Oomens, E. R. Williams, *J. Phys. Chem. A* **2011**, *115*, 2745–2751.
126. O. P. Balaj, D. Semrouni, V. Steinmetz, E. Nicol, C. Clavaguera, G. Ohanessian, *Chem.-Eur. J.* **2012**, *18*, 4583–4592.
127. D. Semrouni, O. P. Balaj, F. Calvo, C. F. Correia, C. Clavaguéra, G. Ohanessian, *J. Am. Soc. Mass Spectrom.* **2010**, *21*, 728–738.

128. R. C. Dunbar, J. D. Steill, N. C. Polfer, J. Oomens, *J. Phys. Chem. A* **2012**, *117*, 1094–1101.
129. J. K. Martens, I. Compagnon, E. Nicol, T. B. McMahon, C. Clavaguera, G. Ohanessian, *J. Phys. Chem. Lett.* **2012**, *3*, 3320–3324.
130. M. Kohtani, B. S. Kinnear, M. F. Jarrold, *J. Am. Chem. Soc.* **2000**, *122*, 12377–12378.
131. M. Kohtani, M. F. Jarrold, S. Wee, R. A. J. O'Hair, *J. Phys. Chem. B* **2004**, *108*, 6093–6097.
132. J. S. Klassen, S. G. Anderson, A. T. Blades, P. Kebarle, *J. Phys. Chem.* **1996**, *100*, 14218–14227.
133. P. Wang, C. Wesdemiotis, C. Kapota, G. Ohanessian, *J. Am. Soc. Mass Spectrom.* **2007**, *18*, 541–552.
134. M. Benzakour, M. Mcharfi, A. Cartier, A. Daoudi, *J. Mol. Struct. Theochem.* **2004**, *710*, 169–174.
135. B. A. Cerda, S. Hoyau, G. Ohanessian, C. Wesdemiotis, *J. Am. Chem. Soc.* **1998**, *120*, 2437–2448.
136. M. M. Kish, C. Wesdemiotis, G. Ohanessian, *J. Phys. Chem. B* **2004**, *108*, 3086–3091.
137. C. H. S. Wong, N. L. Ma, C. W. Tsang, *Chem. Eur. J.* **2002**, *8*, 4909–4918.
138. K. Rajabi, E. A. L. Gillis, T. D. Fridgen, *J. Phys. Chem. A* **2010**, *114*, 3449–3456.
139. B. Yang, R. R. Wu, N. C. Polfer, G. Berden, J. Oomens, M. T. Rodgers, *J. Am. Soc. Mass Spectrom.* **2013**, *24*, 1523–1533.
140. E. A. L. Gillis, K. Rajabi, T. D. Fridgen, *J. Phys. Chem. A* **2009**, *113*, 824–832.
141. Y.-w. Nei, T. E. Akinyemi, C. M. Kaczan, J. D. Steill, G. Berden, J. Oomens, M. T. Rodgers, *Int. J. Mass Spectrom.* **2011**, *308*, 191–202.
142. C. M. Kaczan, A. I. Rathur, R. R. Wu, Y. Chen, C. A. Austin, G. Berden, J. Oomens, M. T. Rodgers, *Int. J. Mass Spectrom.* **2015**, *378*, 76–85.
143. E. Shammel Baker, J. Gidden, A. Ferzoco, M. T. Bowers, *Phys. Chem. Chem. Phys.* **2004**, *6*, 2786–2795.
144. M. T. Rodgers, P. B. Armentrout, *J. Am. Chem. Soc.* **2000**, *122*, 8548–8558.
145. B. A. Cerda, C. Wesdemiotis, *J. Am. Chem. Soc.* **1996**, *118*, 11884–11892.
146. B. Yang, M. T. Rodgers, *Phys. Chem. Chem. Phys.* **2014**, *16*, 16110–16120.
147. P. Wang, M. J. Polce, G. Ohanessian, C. Wesdemiotis, *J. Mass Spectrom.* **2008**, *43*, 485–494.
148. N. Russo, M. Toscano, A. Grand, *J. Phys. Chem. B* **2001**, *105*, 4735–4741.
149. Z. Yang, M. T. Rodgers, *Phys. Chem. Chem. Phys.* **2012**, *14*, 4517–4526.
150. A. L. Lehninger, *Biochemistry, The Molecular Basis of Cell Structure and Function*, Worth Publishers, Inc., New York, 1977.
151. Z. Yang, M. T. Rodgers, *Int. J. Mass Spectrom.* **2005**, *241*, 225–242.
152. Z. Yang, M. T. Rodgers, *J. Am. Chem. Soc.* **2004**, *126*, 16217–16226.
153. Z. Yang, M. T. Rodgers, *J. Phys. Chem. A* **2006**, *110*, 1455–1468.
154. H. Wincel, *J. Am. Soc. Mass Spectrom.* **2012**, *23*, 1479–1487.
155. H. Wincel, *J. Am. Soc. Mass Spectrom.* **2014**, *25*, 2134–2142.